Received: 6 July 2021 | Accepted: 25 August 2023

DOI: 10.1002/nsg.12270

Near Surface Geophysics EAGE EUROPEAN ASSOCIATION OF GEOSCIENTISTS & ENGINEERS

ORIGINAL ARTICLE

Integration of in-mine seismic and GPR surveys to gain advanced knowledge of Bushveld Complex orebodies

Emmanuel O. Onyebueke[1] | **Musa S. D. Manzi**[1] | **Moyagabo K. Rapetsoa**[1] | **Thabang Kgarume**[2] | **Michael Westgate**[1] | **Raymond J. Durrheim**[1] | **Michelle Pienaar**[3] | **Mpofana Sihoyiya**[1] | **Mvikeli Mpofu**[2] | **Michael Van Schoor**[2] | **Phumlani Kubeka**[4]

[1]School of Geosciences, University of the Witwatersrand, Johannesburg, South Africa

[2]Department of Physics, Council for Scientific and Industrial Research, Johannesburg, South Africa

[3]Mandela Mining Precinct, Johannesburg, South Africa

[4]Royal Bafokeng Platinum Mine, Rustenburg, South Africa

Correspondence
Emmanuel O. Onyebueke, University of the Witwatersrand, Johannesburg, South Africa.
Email: Emmanuel.onyebueke.o@gmail.com

Funding information
Council for Scientific and Industrial Research (CSIR); Mandela Mining Precinct, South Africa and the University of the Witwatersrand (Seismic Research Centre); Centre of Excellence for Mineral and Energy Resource Analysis (CIMERA)

Abstract
Improving the exploration of deep-seated mineral deposits and assessing the stability of the mine pillars require that geophysical techniques are deployed in a fast and cost-effective manner with minimal environmental impact. This research presents results from in-mine reflection seismic experiments and a ground penetrating radar (GPR) survey conducted at the Maseve platinum mine, South Africa. The research aims to develop and implement methods to image platinum group metal (PGM) deposits and geological structures near mine tunnels and assess the stability of pillars. The seismic experiments were conducted using a sledgehammer source (10 lb), conventional cabled geophones (14 Hz), and a landstreamer with 4.5 Hz vertical component geophones. The GPR survey was conducted using a Noggin 500 GPR system with 500 MHz centre frequency. An image of the underlying orebody and geological structures down to 100 m from the mine tunnel floor (~500 m below ground surface) was produced. We correlated the coherent reflections beneath the tunnel floor with a known Upper Group (UG2) PGM orebody. The final seismic section shows that the UG2 mineralisation is dissected by near-vertical dykes, faults and fractures. These structures, faults in particular, are interpreted to have been active post-mineralisation, implying that they may have contributed to the current complex geometry of the deposit. Four GPR profiles were collected around a stability pillar adjacent to the seismic lines. The radargram sections were processed to improve the signal-to-noise ratio (S/N). The results show different patterns of fracturing and stress-induced structures. These fractures were shown to be sub-vertical and, possibly, constitute complex micro-structures within the pillar, which could compromise the pillar stability and integrity. The study demonstrates that in-mine seismic and GPR surveys can be cost-effective and valuable for mineral exploration.

KEYWORDS
data processing, GPR, mining, near-tunnel floor, reflection seismic

INTRODUCTION

Mineral exploration relies on the application of advanced geophysical techniques to refine the search for mineral deposits and mine planning (Malehmir et al., 2012, 2017; Manzi et al., 2012, 2020; Stevenson et al., 2003). The seismic method has been well proven as an effective tool for mineral and hydrocarbon exploration, geoengineering, seismic risk assessment, and environmental and hydrogeological investigations (Brodic et al., 2017; Onyebueke et al., 2018, 2020; Manzi et al., 2020). The reflection seismic method provides information about subsurface structures with the advantage of deeper penetration depth and higher resolution compared to other geophysical techniques (Yilmaz, 2001; Malehmir et al., 2012; Manzi et al., 2012, 2019, 2020; Westgate et al., 2020).

The past few years have witnessed an increase in research activity towards in-mine seismic experiments and the utilization of value-added technology in assessing the excavation face and hangingwall stability using ground penetrating radar (GPR) and thermal imagery. These geophysical methods employ combinations of specific acquisition, processing and interpretation techniques in both shallow and deep hard-rock mining environments to improve orebody and structural imaging (Malehmir et al., 2012, 2017; Manzi et al., 2012, 2020; Brodic et al., 2021). The integration of these innovative approaches can nurture new ideas on how the in-mine infrastructure (shafts, boreholes and developmental tunnels) can be utilized to design geophysical experiments. The integrated geophysical approach could provide fresh insights with respect to improving the image of the subsurface geology for mine development and expansion.

Despite various innovative seismic data acquisition approaches in the recent years, numerous difficulties have been encountered with in-mine seismics. The difficulties include noise interference during in-mine data acquisition from electrical infrastructure, mine vehicles, rock blasting and crushing. Several research centres across the world (such as Smart Exploration in Europe, the Seismic Research Centre in Africa, and Metal Earth in Canada) have launched innovative initiatives to tackle these challenges. However, these tools are still under-utilized by South Africa's hard-rock mining industry.

Deep mining in South Africa is characterized by two fundamental challenges: how to optimize the extraction of ore deposits; and ensuring mine safety. The South African Mining Extraction Research, Development and Innovation (SAMERDI) programme established an Advanced Orebody Knowledge (AOK) theme to tackle these issues. Most research is conducted by teams at the University of the Witwatersrand (Wits), University of Pretoria (UP), the Council for Scientific and Industrial Research (CSIR) and the Mandela Mining Precinct (MMP). AOK's goals are to develop and acquire technologies and techniques that will be used to obtain information around the mining tunnels and ahead of the mining face and assess the stability of the hanging wall and pillars. Seismic modelling and innovative in-mine seismic surveys are important components of this endeavour to reduce drilling and exploration costs, maximize mine safety, find new brownfield ore bodies and increase the life of mines (Westgate & Manzi, 2017; Westgate et al., 2020). The AOK project also seeks to advance LiDAR, GPR and thermal imagery technology to provide more detail of the discontinuities and locations of loose block of rocks within the supporting pillars (e.g., joints and fractures), which could cause rockfalls and pillar instability.

The seismic experiments involved both passive surveys (sensors deployed on the Earth's surface) and active surveys (sensors both on the surface and in tunnels). In this paper, we focus on the in-mine active seismic experiments using a seismic landstreamer system, sledgehammer and cabled geophones inside the mine tunnel and a GPR survey around the reference pillar (known as 'Michelle's pillar'). Our experiments were conducted in tunnels excavated within the Merensky Reef (MR) in order to map the structure of the underlying Upper Group orebody (UG2), which is high-grade platinum group metal (PGM) ore deposit. The GPR was used to scan Michelle's pillar to gain an overall understanding of the discontinuities within the pillar's interior.

SITE LOCATION AND BACKGROUND GEOLOGY

The study area is located within the Western Lobe of the Bushveld Complex (BC). Maseve mine is ~38 km NW of Rustenburg and ~10 km south of the Pilanesberg Alkaline Intrusive Complex in the North West Province, South Africa (Figure 1a). The BC is the world's largest host of PGMs, vanadium and chromium commodities (Magson et al., 2018) (Figure 1a,b). The complex has been mined for decades and plays a key role in South Africa's economy. The presence of complex geological structures, such as faults, dyke swarms, iron-rich ultramafic pegmatites (IRUPs) and potholes, renders the seismic imaging and full exploitation of these economic platinum-bearing horizons (known as reefs) challenging (Manzi et al., 2020). These make the Maseve mining environment an ideal site to conduct such seismic experiments. The mine is located within the Western Bushveld joint venture project area (Royal Bafokeng Platinum [RBPlat], 2020) (Figure 1a).

The BC is a layered igneous province with an area extent of 65,000 km^2 and thickness of 5–10 km (Figure 1a,b). It spans 450 km east–west and 350 km north–south (Campbell, 2011; Kawohl & Frimmel, 2016; Bachmann et al., 2018; Magson et al., 2018). The BC is Paleoproterozoic in age, dated ~2.06 Ga. The rock compositions range from mafic to ultramafic, felsites and granites, which formed on the stable Kaapvaal and Zimbabwe cratons towards the north-eastern part of South Africa (Magson et al., 2018). The complex is divided into five lobes, namely the Northern, Southern (or Bethal), Western, far Western and Eastern. At the current levels of erosion, it consists of three lobes, the Northern, Eastern and Western Lobe (Cawthorn et al.,

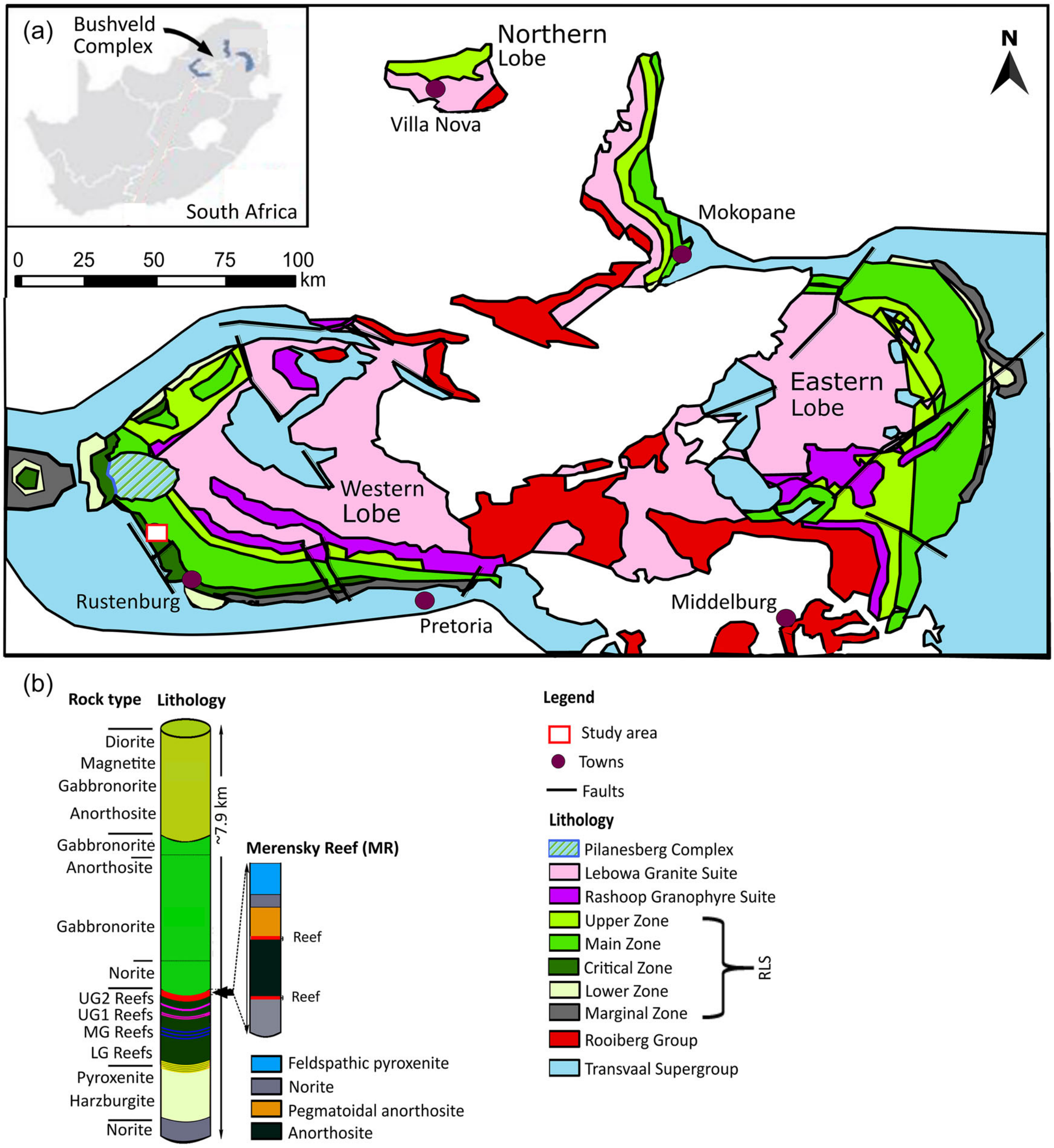

FIGURE 1 (a) The geology of the three major lobes and the three main suites of the Bushveld Complex, the index on the top left is the South African outline map indicating the position of Bushveld Complex (modified after Kinnaird, 2005 and Manzi et al., 2019). (b) General stratigraphy of the Rustenburg Layered Suite (RLS) and the schematic enlargement of the Merensky Reef. The Suite is estimated to be ~8 km thick (Kawohl & Frimmel, 2016; Magson et al., 2018); note that the figure is schematic and not drawn to scale.

2002) (Figure 1a). The BC has been further subdivided into the Rooiberg Group, Lebowa Granite Suite and the Rustenburg Layered Suite (RLS).

The RLS was emplaced at 2.06 ± 0.0026 Ma and cooled by 2.05 ± 0.0037 Ga (Zeh et al., 2015; Oppermann et al., 2017). The RLS succession is subdivided into the Marginal, Lower (LZ), Critical (CZ), Main and Upper zones (UZ), which are categorized by their unique igneous intrusive layering (Figure 1b). The Upper Group of the RLS CZ hosts the largest concentration of these PGMs (platinum, palladium, iridium, rhodium, osmium and ruthenium). The most important orebodies are the Upper Group (UG2) chromitite reefs, the MR and Platreef mineralization in the Northern Lobe. The stratigraphic column shown in Figure 1b illustrates the positioning of the UG2 relative to the MR, (Kinnaird, 2005; Campbell, 2011; Magalhães et al., 2018). The Merensky and UG2 reefs dip ~5°–15° N and also contain sulphides, which host the PGMs, gold and varieties of copper and nickel minerals (Kinnaird, 2005; Magalhães et al., 2018). The surface geology comprises the lower portion of the RLS with 14 major chromitite seams and numerous less developed seams (Oppermann et al., 2017) (Figure 2a–c) (RBPlat, 2020). The CZ

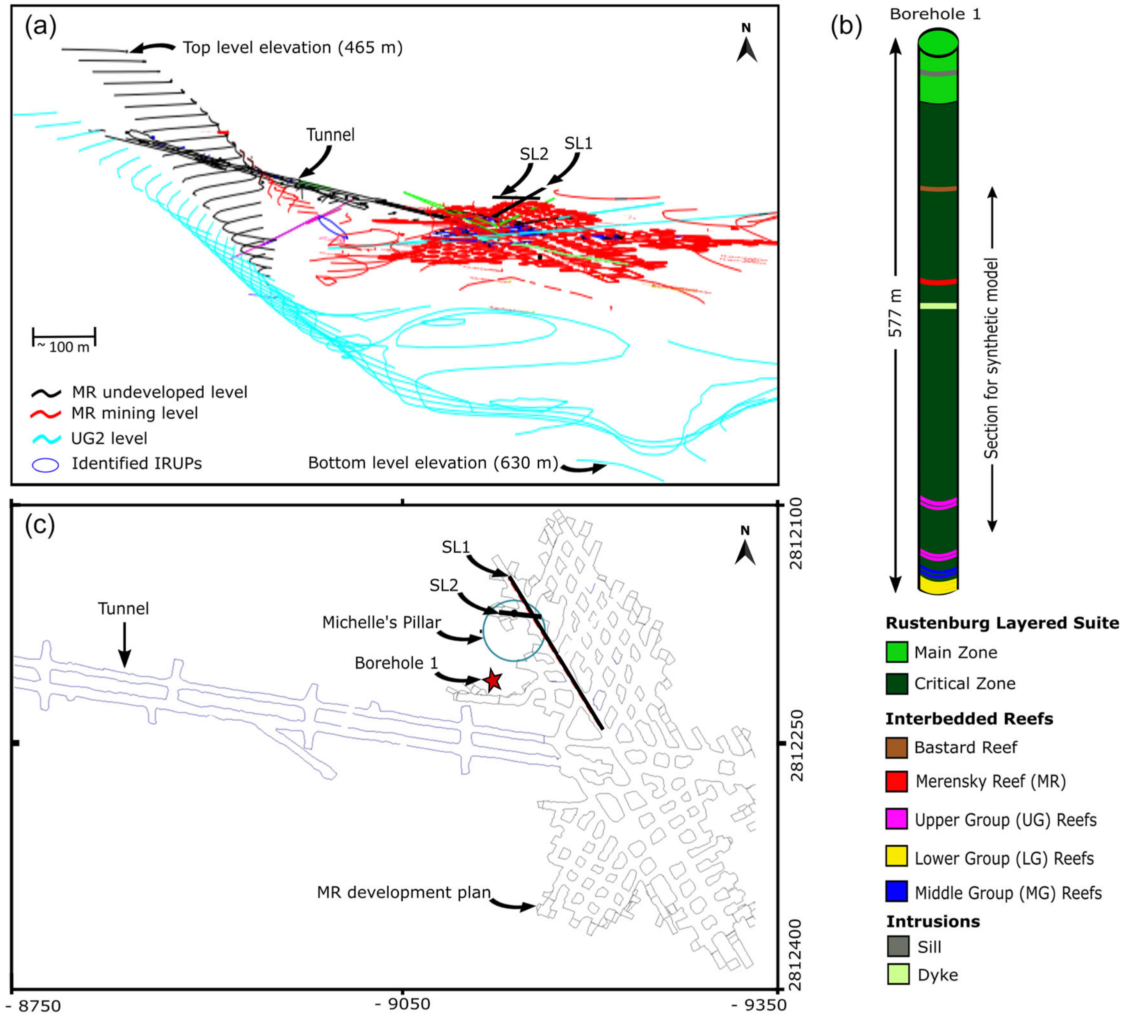

FIGURE 2 (a) Depth contours of the Merensky Reef (MR) and Upper Group 2 (UG2) showing the mining levels and identified iron-rich ultramafic pegmatite (IRUP). (b) Underground mining plan showing the locations of the seismic line 1 (SL1) and 2 (SL2), the Borehole 1 and Michelle's pillar, (c) borehole lithology in the mine area (note that the figure is schematic and not drawn to scale but to show rock layering). Note that the elevation is above sea level.

of the RLS in this region comprises cyclic units of mafic cumulate rocks ranging from harzburgite to orthopyroxenite composition in the LZ, whereas the UZ includes orthopyroxenite, norite and anorthosite (Schoenberg et al., 1999; Barnes et al., 2004). The enrichment of PGMs in this area has been explained by a variety of models that include the mixing of sulphide-rich horizons and large amounts of silicate melts in either a closed or open magma chamber system (Kinnaird, 2005; Kawohl & Frimmel, 2016; Magalhães et al., 2018).

The mining development in the area is currently on the MR level, which is regarded as a uniform package of chromitite- and sulphide-bearing orthopyroxenite hosted by norite and/or anorthosite (Chistyakova et al., 2019) (Figure 2a–c). The thickness of this reef ranges from 4 cm to 4 m. Chistyakova et al. (2019) subdivided the MR into four horizons (MR-1–MR-4). The UG2 reef occurs between 15 m and 100 m below the MR and comprises a 0.7–1.2 m thick (main) chromitite seam with 2–4 m thick hangingwall chromitite (Campbell, 2011). Underlying the UG2 in the area are UG1, Middle Group and Lower Group chromitite seams. The orebodies in the study area are affected by major faults (e.g., Rustenburg Fault) and a network of north to northeast trending dolerite and diabase dyke swarms of Waterberg and Karoo age (Campbell, 2011).

GEOPHYSICAL METHODS

Seismic method and synthetic modelling

Refraction and reflection seismic surveys were conducted to image the rock mass beneath the mine's tunnel floor. For survey design purposes, and subsequent interpretation, seismic responses of targeted

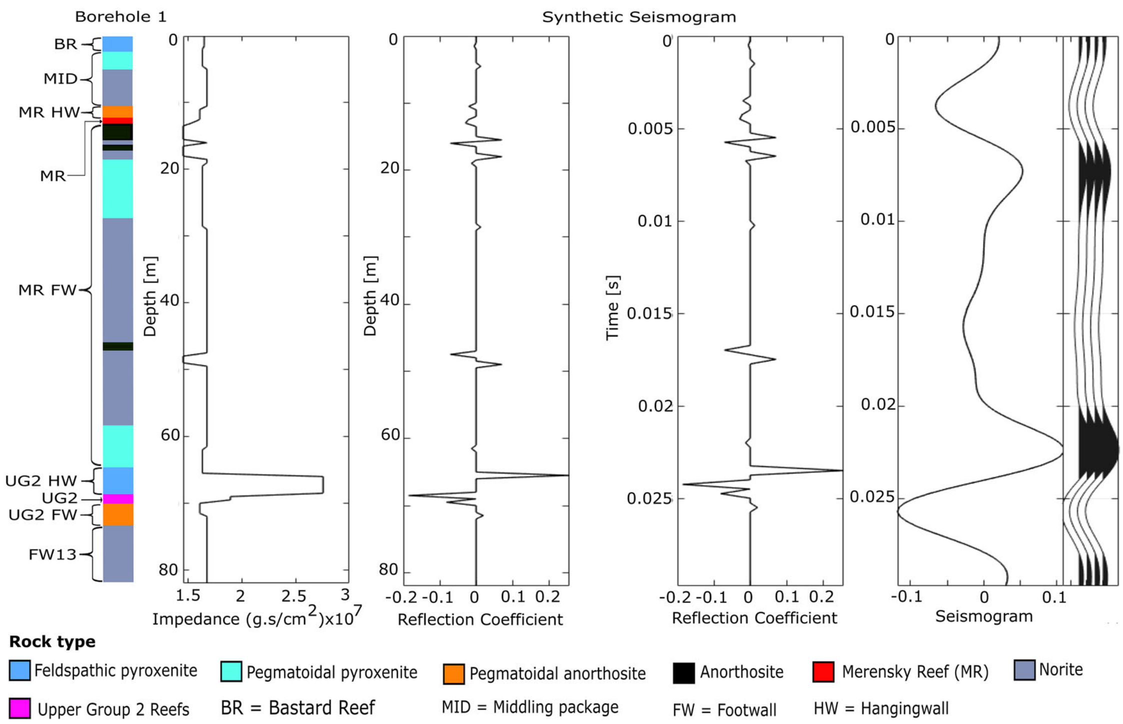

FIGURE 3 Synthetic seismogram plot using laboratory physical property measurements of Borehole 1 rock and ore samples.

horizons would be evaluated via forward modelling. Ore deposits in the BC typically exhibit a contrast in seismic impedance with their host rocks due to variation in rock densities and seismic velocities, which is quantified by the reflection coefficient (Campbell, 2011; Manzi et al., 2019). The impedance contrasts in the area are attributed mostly to the litho-structural boundaries (dykes, faults and IRUPs) and magmatic layering. Previous research conducted in the study area using reflection seismic data and synthetic modelling drilled cores had reported the range of P-wave velocities in the BC between 5500 and 6800 m/s (Trickett et al., 2009; Campbell, 2011; Scheiber-Enslin & Manzi, 2018; Manzi et al., 2019). Generally, the CZ is characterized by alternating sub-horizontal strata of anorthosites and norites, and ultramafic pyroxenites with intercalated chromitite seams, which include the targeted pyroxenite–chromitite UG2 package. The Merensky and UG2 reefs have estimated average P-wave velocities of 6400 m/s and 6800 m/s and density values of 2.9 g/cm^3 and 3.15 g/cm^3, respectively (Campbell, 2011; Manzi et al., 2019). The reflection events in the CZ are expected at the interface between the low-density anorthosite (2.78 g/cm^3), which hosts the MR and the higher density pyroxenite (4.3 g/cm^3), which host the UG2. The UG2 is approximately 15–100 m below the MR platform. The synthetic seismogram in Figure 3 was calculated using laboratory ultrasonic P-velocity and density measurements of the host rocks and ore samples obtained at Maseve mine starting from the Bastard Reef (Table 1).

The physical property estimations were performed with the average of 10 measurements of each rock type, and the results obtained are consistent with earlier report at the same site (Campbell, 2011). The seismogram was estimated using a minimum phase Ricker wavelet centred at 100 Hz and 0.25 ms sampling interval to resemble the expected input wavelet of a hammer source.

Seismic data acquisition

The in-mine seismic experiments were conducted along four different 2D profiles around the reference pillar, of which two lines are presented in this study (Figure 2a,b). A conventional seismic landstreamer coupled with 24 receivers (4.5 Hz) connected to a Geometrics Geode seismograph was deployed along the tunnel floor across SL1 and SL2. The landstreamer was attached on a car with a non-stretchable cargo belt. Table 2 summarizes the acquisition parameters for SL1 and SL2. The choice of the landstreamer was justified in this study due to the tunnel accessibility and better receiver-ground coupling. Several acquisition trials were performed to observe the effect of rebounds and tunnel echo. A sledgehammer (10 lb) was used as the seismic source. To minimize noise, data acquisition was stopped whenever mine trucks or heavy machinery operated nearby.

To improve the signal-to-noise ratio (S/N), a vertical stack of five hammer blows were taken at every source station. We acquired the data using 500 ms (SL1) and

TABLE 1 Average values of physical property measurement of Bushveld Complex rocks.

Rock type	P-wave velocity (m/s)	Density (kg/m^3)
Merensky Reef (orthopyroxenite)	5950	2745
Upper Group 2 (chromitite)	6118	4293
Anorthosite	5530	2948
Pegmatoidal anorthosite	5088	2851
Norite	5667	2951
Feldspathic pyroxenite	5400	3000
Pegmatoidal pyroxenite	5900	2700

TABLE 2 Acquisition parameters and geometries used in the in-mine underground tunnel seismic experiments.

Parameters	Values	
Seismic lines	SL1	SL2
Profile length (m)	115	25
Seismogram	Geometric Geode	
Geophone (Hz)	4.5	4.5
Source	10 lb sledgehammer	
Receiver number	24	24
Receiver spacing (m)	5	1
Shot spacing (m)	5	2
Record length (ms)	500	150
Sampling interval (ms)	0.25	
Vertical stacks	5	
Min/max offset (m)	2.5/120	1/24
Max CMP fold	24	12
Survey direction	Strike direction	Up dip direction

Abbreviation: CMP, common midpoint.

150 ms (SL2) recording time with 0.25 ms sampling interval. The shot points were located in between every two receivers. The asymmetrical split-spread yielded a common midpoint (CMP) subsurface spacing of 2.5 m in SL1 and 0.5 m in SL2 with nominal folds of 12 and 6, respectively (Levande et al., 1994; Minato et al., 2012; Onyebueke et al., 2020). Two offset shots were taken at 2.0 m and 5.0 m from the end of each line, respectively. There were significant challenges in acquiring seismic data along the mine tunnel, which include obtaining accurate elevation measurements for each geophone and shot position, the flooded areas of the tunnel that made it difficult to place the receivers, difficulty in planting and obtaining tight coupling of the geophones on a fresh rough bedrock surface and high humidity level and poor air ventilation.

Seismic data analysis

Figure 4 shows examples of raw and processed shot gathers with associated amplitude spectra. The data were recorded using a high sample rate of 0.25 ms for useful signal versus mining noise bandwidth experimentation purposes. However, as can be seen from Figure 4a, the strong mining noise, inevitable at these sites, dominates the signal using such fine sampling where clear first breaks cannot be noted. The situation improves after processing (Figure 4b) where a shallow event marked R1 becomes prominent. Similar situation can be seen for the second line indicated in Figure 4c,d. The average frequency (F_a) of the useful signal in our data is ~100–140 Hz, consistent with a same nature source (impact hammer) used in Brodic et al., 2017 (Figure 4a,c). The 'NS' was due to high energy content at the vicinity of the impact source, whereas 'AS' was caused by loose/malfunctioning geophones. Preliminary processing reduced the amplitude of the near-source wave and high-frequency signal (>200 Hz) visible in the shot gathers. The coherent events approximately at 25–50 ms (labelled R1) (Figure 4b,d) could be the expected reflections from the pyroxenite–chromitite UG2 package, approximately 50–100 m below the tunnel floor. This is

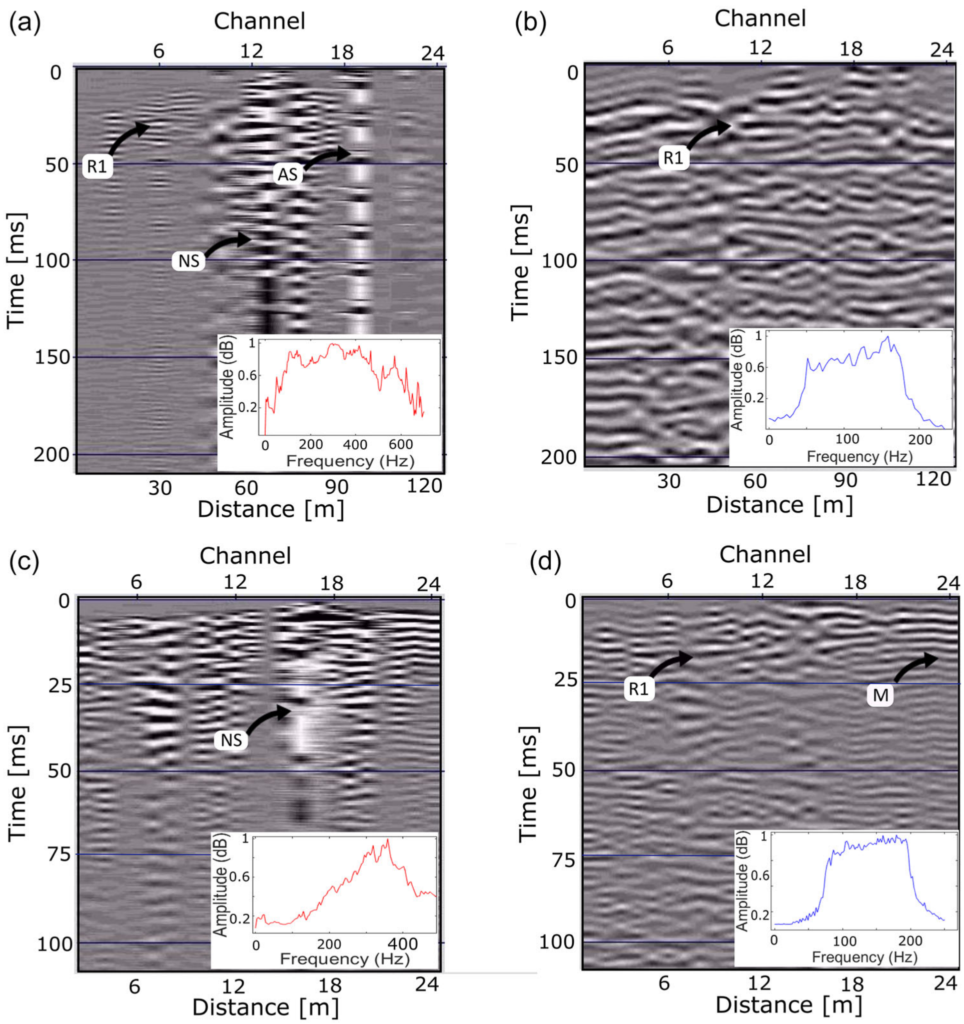

FIGURE 4 Shot gathers after different processing steps along seismic lines 1 (SL1) and 2 (SL2). Part (a) shows SL1 raw shot gather indicating some seismic events and part (b) shows SL1 shot gather after bandpass frequency filter, AGC, FK filter and spiking deconvolution. Parts (c) and (d) show the same steps as in parts (a) and (b) on SL2. The inserts on the bottom right are the frequency spectra of the seismic shot gather events. R1-possible reflection. AS, amplitude spikes; NS, near-source high-amplitude waves.

supported by the synthetic results shown in Figure 3. The events (labelled M) observed between 50 ms and 200 ms are likely reverberations (Figure 4d).

Seismic data processing and results

The traces were normalized with respect to the average amplitude of the entire shot gather, and dead traces were removed. The pre-processing involved bandpass frequency filtering (60–70–180–200 Hz) with 50 ms AGC to compensate the amplitude variation and loss of energy with depth (Figure 4b,d). To enhance the coherent events that might be reflected from the targeted horizon and improve the S/N, we adopted a conventional reflection seismic processing workflow. The processing steps are listed in Table 3. These include geometry set-up, trace edits and normalizations, first break picking, refraction statics, frequency bandpass filtering, pre-stack deconvolutions; standard CMP sorting, velocity analysis, normal moveout correction (NMO); stacking, migration and time-to-depth conversion.

The number of CMP gathers across SL1 and SL2 were 61 and 48, respectively. The significant step in improving the quality of reflections relies on picking P-wave first arrivals and using them for refraction static correction purposes (Figure 5a–d). The tomograms were generated using the simultaneous iterative reconstruction technique (SIRT). The SIRT algorithm estimates the theoretical traveltime from the observed datasets and finds a velocity model that reduces the error between them to a minimum. The advantage of this algorithm is the ability to constrain the inversion using acquisition geometries and the estimated apparent velocities of the first break picks to generate the final P-wave velocity model (Figure 5c,d). The vertical extent of the starting

TABLE 3 Data processing steps and parameters.

Processing steps	Parameters
Geometry setup	Trace header updated with observer's report
Trace normalization	With respect to the average amplitude of the entire shot gathers
Trace editing	Removed dead and noisy traces
AGC	Using 50 ms window length
Brute stack	Initial constant velocity range of 3500–6500 m/s
First break pick and velocity inversion	Velocity range of 3000–6000 m/s with 0.01 misfit
Muting	Surgical muting of the first arrivals
Static correction	Using refraction velocity at 536 m floating datum
Spiking deconvolution	Deconvolution of 30 ms autocorrelation with 5 ms length
Bandpass frequency filter	Butterworth: 60–70–180–200 (Hz)
fk filter	3000–8000 m/s
CMP/CDP sorting	61 and 48 gathers for L1 and L2
Residual static correction	Near-surface constant statics
NMO and stacking	Using interactive constant velocity panel and semblance with velocity range of 3500–6800 m/s (45% stretch)
Migration	2D Kirchhoff migration algorithm with interval velocity range of 3500–6800 m/s
Time-depth conversion	Using interval average velocity range of 3500–6800 m/s

Abbreviations; CMP, common mid-point; NMO, normal moveout.

velocity models for SL1 and SL2 ranges from 0 m to 40 m with 0.4 m cell size and P-wave velocity range of 3000–6800 m/s. The inversion was based on iteration model (the results were obtained after 20 iterations) with a defined data variance of 0.01 (misfit), the permissible threshold of 0.001 and a maximum defined change of 50% as an input parameter.

The filtered shot gathers were sorted into CMP for velocity analysis. The velocity analysis was based on interactive constant velocity picks and semblance recognition. Figure 5e,f shows the final stacked reflection sections after applying bandpass frequency filter, *fk* filter, deconvolution and subsequent velocity analysis (Figure 4a–d). We applied surface-consistent static corrections to compensate for the elevation and short–long wavelength variations. The CDP gathers were 45% muted after NMO correction to account for NMO stretching (45% stretch). Given that our seismic lines are located inside a tunnel within a solid rock space, we assume that the reflected energy seen in the final stacked sections originates from within our stacking plane. We assume that off-the-plane contributions would be handled by the Kirchhoff time migration algorithm used. However, we are fully aware that a proper separation of in- versus off-the-plane reflection contributions would require 3D time/depth migration using true acquisition geometry, presently unavailable. The data were migrated using the Kirchhoff algorithm and converted to depth using the stacking velocity model, which ranges from 3500 m/s to 6800 m/s with 200 m/s velocity interval.

The GPR data were acquired using the Noggin 500 GPR system (Lee at el., 2021; Yang et al., 2021) with a centre frequency of 500 MHz. The acquisition procedures involve moving the antenna along the sidewall of the reference pillar (Figure 6a,b). A total of four lines (GPRL1 [8 m], GPRL2 [6.5 m], GPRL3 [11.4 m] and GPRL4 [6.6 m]) were acquired around Michelle's pillar (Figure 6b). Common-offset reflection survey mode was used for data acquisition with 0.025 m trace spacing, 0.2 ns sampling rate and 120 ns listening time. To improve the S/N ratio, eight vertical radargram were stacked at each sampling point (Figure 6c–f). The GPR sections in Figure 6c–f show radar traces (radargram) plotted against time and distance across the sidewall of Michelle's pillar (Figure 6a,b). The *x*-axis represents the distance along the survey line, whereas the *y*-axis represents the traveltime of the radar pulses. The radar profiles acquired in the surveyed area show several reflection events, which exhibited an average velocity of 0.1 m/ns as well as presence of background noise.

The GPR data processing involved correcting the radargram to zero time (time delay), applying a time-varying spherical and exponential gain to correct for the spherical spreading and intrinsic attenuation of the signal, and a bandpass filter (200–800 MHz) to attenuate the unwanted frequency components. The dominant frequency is approximately 400 MHz. Background removal (subtracting mean) filter was used to enhance the subvertical reflectors as well as suppress the background noise and the direct arrivals (Figure 6g–j). The GPR

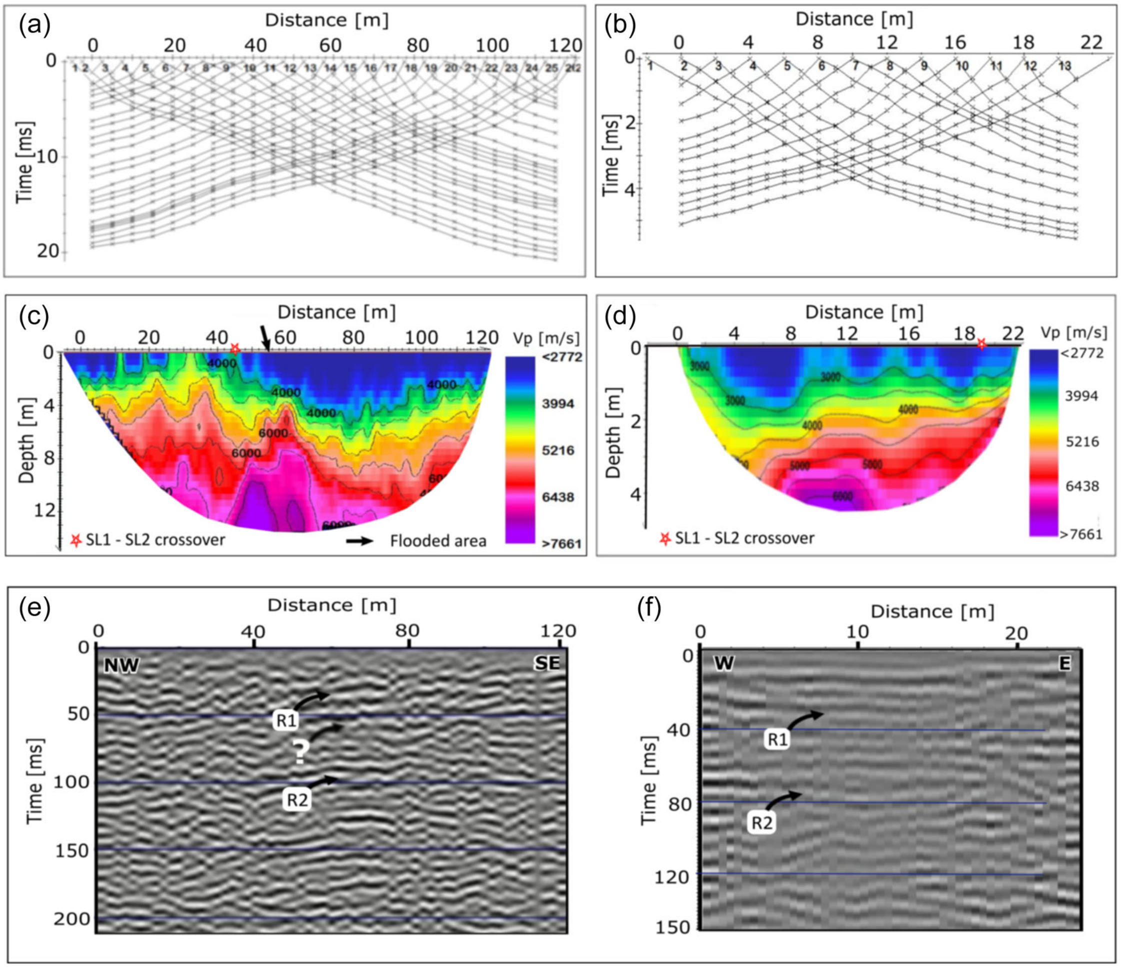

FIGURE 5 Parts (a) and (b) are the seismic line 1 (SL1) two-way traveltime plot and tomogram, respectively; parts (c) and (d) are the seismic line 2 (SL2) two-way traveltime plot and tomogram, respectively. (e) Stacked-time section of SL1 indicating possible Upper Group 2 (UG2) reflection package (R1) and possible reverberation (R2). (f) Stacked-time section of SL2 (this line is short and does not provide adequate reflection information for further interpretation).

profiles were migrated and converted to the distance of penetration with a constant velocity of 0.1 m/ns. The migration collapses the diffractions and allows the geometries of the linear structural features on the pillar to be delineated.

INTERPRETATION

This study aimed to demonstrate how in-mine geophysical surveys can produce subsurface images of the rock mass near the excavation surface and the interior of mine pillars as well as provide insight about the complex geological structure of the orebody in the area. A site reconnaissance was conducted upon our arrival, consisting of equipment testing to observe different geophone responses (4.5, 14, 45 and 100 Hz resonance frequencies) and planning a cost-effective and successful data acquisition. Campbell (2011) and Manzi et al. (2019) used 2D and 3D reflection seismic data sets and borehole information to provide detailed subsurface images of the BC for mineral exploration. They produced synthetic seismograms using wireline measurements of sonic velocity and density to show that the UG2 and UG1 pyroxenite–anorthosite contacts are the main seismic reflection markers in the area.

The interpretations of the reflection seismic sections in this study are based on coherent event characteristics and comparison with borehole information, synthetic seismograms and previous research results (Campbell, 2011; Manzi et al., 2019) (Figures 7 and 8). The data were acquired in tunnels excavated for the MR exploitation ~500 m below the ground surface (Figure 7a). The main feature belonging to the Upper Group is shown on the reflection seismic sections as a coherent reflection (R1) at shallow depth below the tunnel floor, which we interpreted as UG2 (Figure 7b,c). The strong reflection is due to high acoustic impedance contrast with their

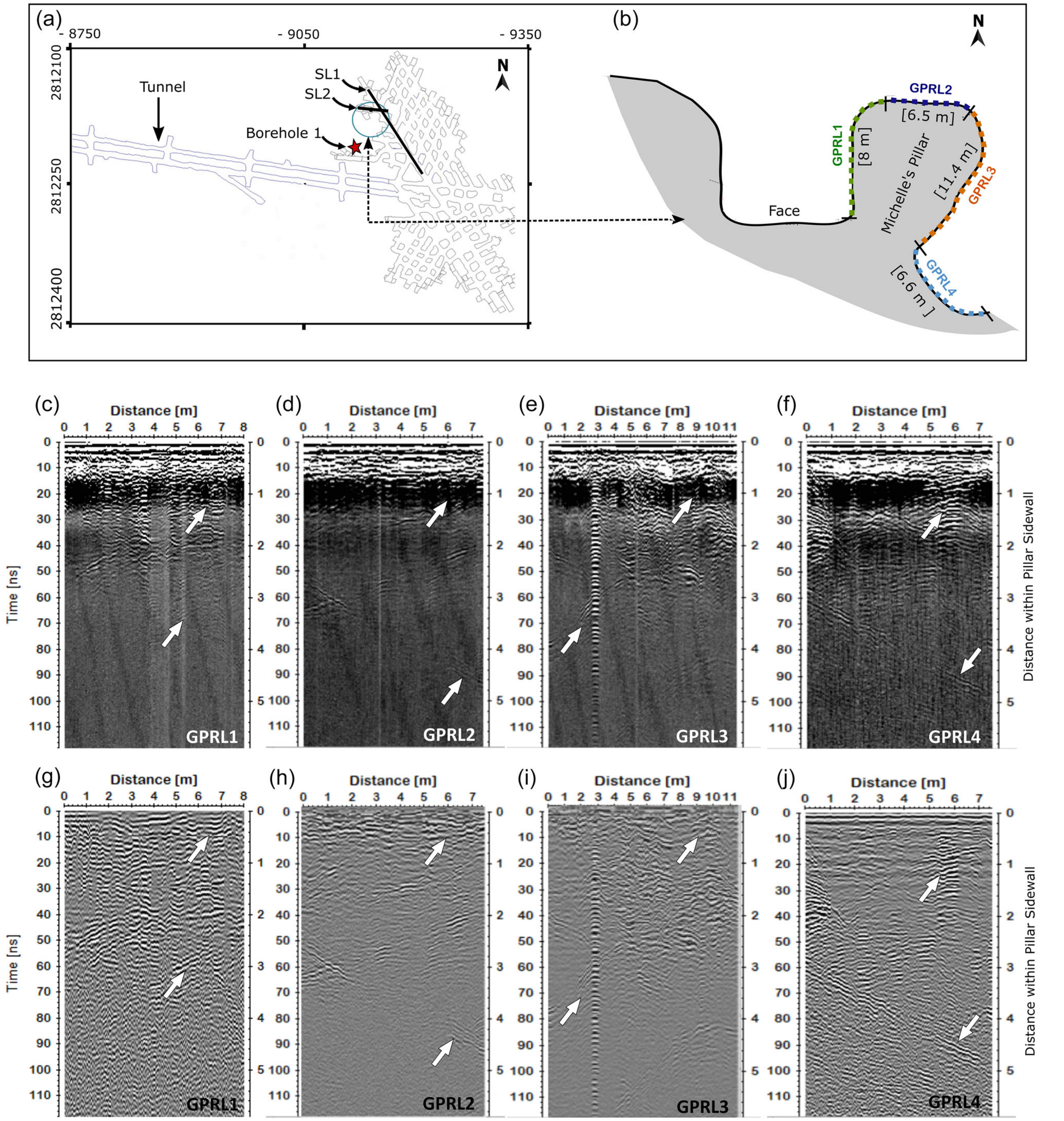

FIGURE 6 Underground mining plan showing the locations of the seismic lines 1 (SL1) and 2 (SL2), the borehole 1 and Michelle's pillar. (b) The enlarged schematic diagram of the reference pillar indicating the positions of the ground penetrating radar (GPR) lines (GPRL1–GPRL4). Parts (c)–(e) and (f) show the unprocessed radargram sections of GPRL1–GPRL4 after delay time removal, respectively. Parts (g)–(j) show the processed radargram sections of GPRL1–GPRL4, respectively (note the significant improvement of the sub-vertical reflectors and background noise removal from the raw radargram sections as pointed out with white arrows).

host rocks (orthopyroxenite and anorthosite), which is comparable with studies by Campbell (2011) and Manzi et al. (2019). The reflector R2 was attributed to multiples as the SL1 profile length and energy source were deemed not capable of reaching such depth. The results correlated well with the synthetic seismogram from the Borehole 1 that intersects this mineralization (Figure 7c). The delineated UG2 exhibits a gentle dip (~10°–15° NW) across the depth section of SL1 (Figure 7d) but was not well resolved in SL2 due to the short profile length. The depth from the survey elevation (tunnel floor) to the underlying UG2 is ~40–100 m, which is in

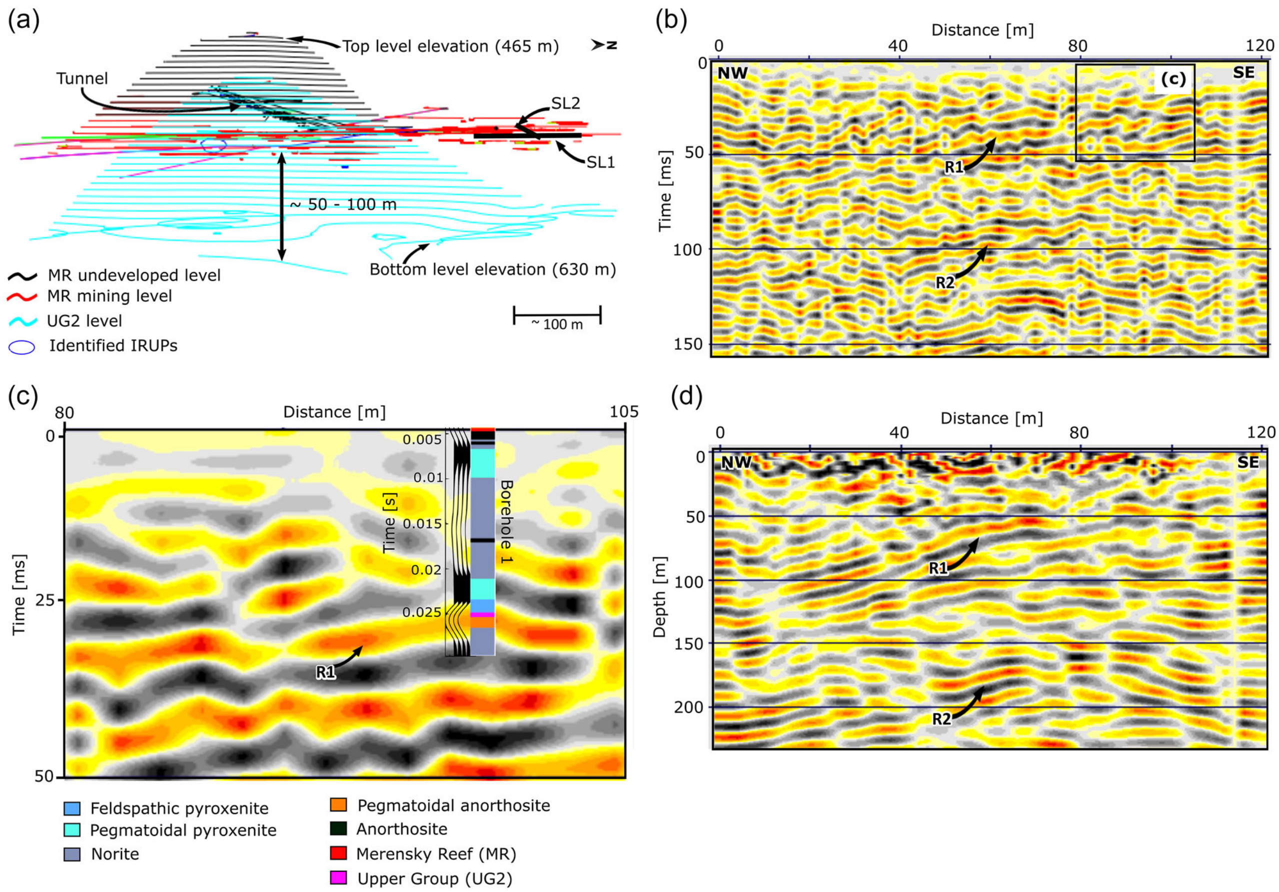

FIGURE 7 (a) Elevation contour of the mineralized Merensky Reef (MR) and Upper Group 2 (UG2) indicating the locations of seismic lines 1 (SL1) and 2 (SL2) (note, IRUP – iron-rich ultramafic pegmatite and the elevation is above sea level.), (b) stacked reflection seismic time-section of SL1 indicating some prominent seismic events (the black rectangular block on top right is an enlarged section of the line shown in part (c)), (c) the enlarged section of SL1 as shown in part (b) with superimposed synthetic model and the corresponding Borehole 1 lithology for comparison, (d) uninterpreted migrated depth section of SL1 (note this section is vertically exaggerated, equivalent to 100 ms). The seismic events R1 and R2 are the suggested UG2 reflection package and possible reverberation.

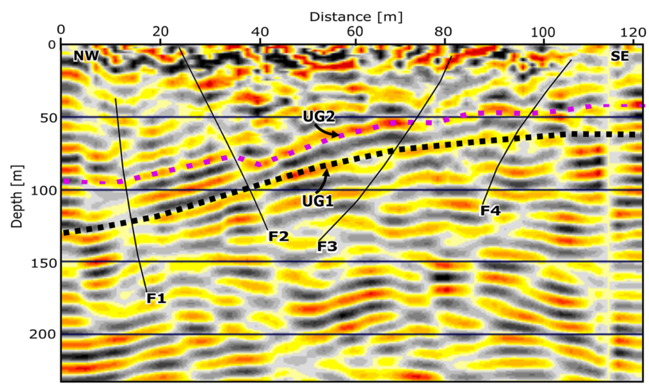

FIGURE 8 Interpreted depth section of seismic line 1 (SL1) indicating the prominent reflection package of Upper Group 2 (UG2) and possible Upper Group 1 (UG1). Note the dotted lines are the R1 reflection package, which is interpreted as the UG2 and UG1 Groups.

agreement with the borehole information. In addition, another relatively strong reflection (~15–40 m below UG2) has been observed, and it could be associated with another potential mineralization (known as UG1) (Figure 8). The observed undulating or dipping reflections shown in the dip section across UG2 could be as a result of faulting and folding commonly found in the BC (Manzi et al., 2020) (Figure 8). The underlying UG2 and UG1 reflection markers and associated faults and fractures discerned between ~40 m and 130 m in Figure 8 confirm and support previous research conducted in the western BC (Campbell, 2011; Manzi et al., 2019).

Maximum penetration depths of about 13 m and 5 m were achieved across SL1 and SL2, respectively, on the refraction tomograms. The low P-wave velocity zone (Figure 9a) observed across SL1 was interpreted as a result of flooded area seen on the surface, and fractured bedrock near the tunnel floor due to mining activities such as rock blasting and excavation. The low P-wave velocity zone between distances 2 m and 8 m in SL2 tomogram (Figure 9b) is attributed to fractures evident on the tunnel floor.

Near Surface Geophysics EAGE EUROPEAN ASSOCIATION OF GEOSCIENTISTS & ENGINEERS

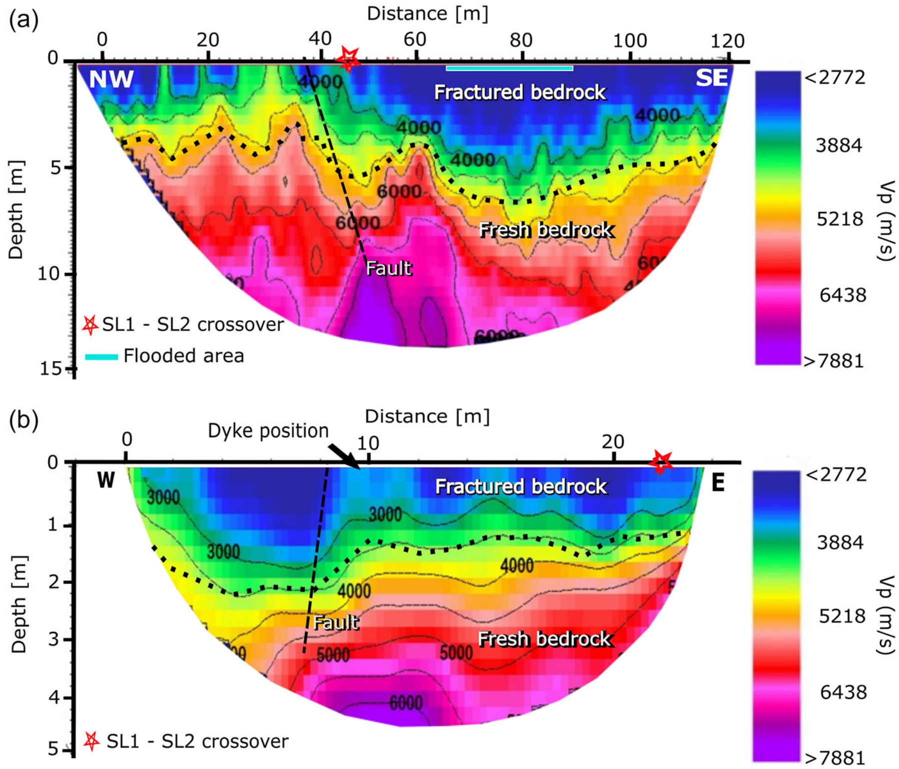

FIGURE 9 Interpretation of tomogram sections along seismic line 1 (SL1) (a) and line 2 (SL2) (b).

Figure 10 shows the merged radargram of GPR lines (GPRL1–GPRL4) acquired around the sidewall of Michelle's pillar. Different fracture patterns and stress-induced micro-strains were observed. The radargrams are dominated by NW–SE and NE–SW striking linear structural features, which could be faults, joints and stress-induced fracture sets. These linear structural features can be observed across the pillar with major stress-induced strains and micro-fractures observed at about 1–3 m distance inside the pillar sidewall across GPRL1, GPRL3 and GPRL4. Sidewall parallel stress-induced micro-fracturing were observed across all the lines conducted around the pillar. A prominent linear structural feature in GPRL2 strikes from 2.0 m to 3.5 m distance inside the pillar sidewall. Complex fracturing is observed in GPRL3 with two prominent linear structures (probably fractures), striking towards the northwest at 1.5–6.0 m distance within the sidewall, with another three striking perpendicularly towards the southeast. The stress-induced micro-fractures in GPRL3 extend to an overlapping distance between GPRL4. Another prominent sub-vertical reflector was also observed in GPRL4, which strikes towards the southeast at 2.5–5.0 m distance within the pillar sidewall. The metal response observed on the GPRL3 section is due to pillar bolt. The interaction of these structures could compromise the stability of this supporting pillar. The difference in the intensity of the fracturing could be ascertained by the degree of electromagnetic wave reflectivity and radargram texture. The observed texture of the radargrams is clearly different across the image of the scanned pillar, which could reflect the degree of fracturing as well as structural compositions (Figure 10). The information from seismically defined known mineralization (UG2), additional potential resources (UG1) and structural styles should be incorporated in the future mine planning and designs. Future drilling could focus on targeting the UG1 mineralization to confirm its existence and assess its economic value.

In future, we plan to improve the quality of the seismic data with different survey designs and use other seismic technologies such as distributed acoustic sensing to image below the tunnel, surface-tunnel recording to image the rock mass between ground surface and tunnel floor and cross-hole tomography to improve structural imaging between boreholes. In addition, with an increase budget, we can also explore more powerful sources that are less manually and labour-intensive and provide deeper penetration. We are also planning to conduct a 3D GPR and thermal image scan across the supporting pillars and the mining face (Riedel et al., 2018).

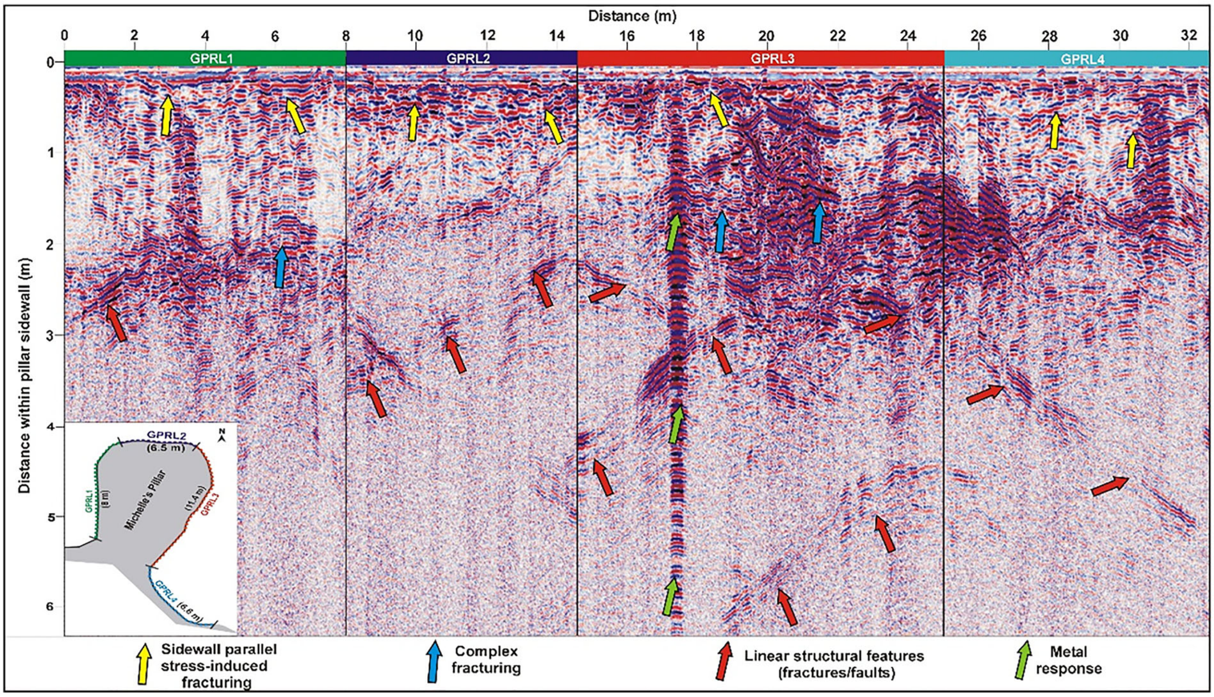

FIGURE 10 Interpreted merged ground penetrating radar (GPR) lines (GPRL1–GPRL4). The index on the bottom left is a schematic diagram of Michelle's pillar with respective positions of the GPR lines. Note the yellow, blue, red and green arrows indicate sidewall parallel stress-induced fracturing, complex fracturing, linear structural features (fractures/faults) and metal response, respectively.

CONCLUSIONS

Pilot in-mine geophysical experiments have been conducted at Maseve mine, Rustenburg, South Africa, to image the platinum orebodies below the mine exploration tunnel (~500 m below ground surface), complex geological structures that complicate mining as well as the interior of the mine pillar. Seismic and GPR methods were employed. The seismic and GPR data were acquired and processed. The initial seismic analysis revealed various seismic events on the raw shot gathers, namely the first P-wave arrivals, surface waves and high-amplitude noise. The data were processed to attenuate unwanted signals and enhance the coherent reflection events arising from the UG2 and UG1 reflectors. The coherent reflected event observed at the shallow depth (<100 m) was attributed to the UG2 pyroxenite–anorthosite packages in the CZ of the Rustenburg Layer Suite. The underlying UG2 reflection markers discerned between 40 m and 100 m confirm and support previous research conducted in the area. The seismic section also exhibits relatively strong reflection at 40–80 m below UG2, which is likely from another mineralized zone. The imaging of this new mineralized zone is important for the mine for future resource enhancement, mine planning and design. Possible subtle faults and fractures (no clear offsets observed) were also delineated by the reflection seismic sections. While we plan to acquire numerous in-mine seismic surveys on the same site, the results from this pilot study are encouraging and will be used as guidelines for future in-mine seismic survey planning and acquisitions. The GPR radargram image of the mine pillar provides a good understanding of discontinuities within the rock mass, particularly the sub-vertical reflectors, linear structural strikes (fractures and faults) and stress-induced micro-fractures. The GPR method is a fast geophysical technique that can complement other geophysical methods in assessing the stability of mine pillars and obtaining information ahead of the mining face that has an impact on excavation integrity.

ACKNOWLEDGEMENTS

Appreciation goes to the Council for Scientific and Industrial Research (CSIR) through Mandela Mining Precinct, South Africa and the University of the Witwatersrand (Seismic Research Centre) for the sponsorship and support. Authors would like to thank the following companies for their support in this project: Thanks to GeoLink, OpenGround Resource Pty and Engineering & Exploration Geophysical Services CC for equipment support; HiSeis Ltd and Globe Claritas for supporting us with the licences for Claritas seismic processing licences; Wits Geophysics Research Team for assistance with data acquisition. Centre of Excellence for Mineral and Energy Resource Analysis (CIMERA) for providing financial support. We would also like to thank the anonymous reviewers for providing constructive criticism, which improved the quality of this work.

DATA AVAILABILITY STATEMENT

The data that support the findings of this study are available on request from the corresponding author. The data are not publicly available due to privacy or ethical restrictions.

ORCID

Musa S. D. Manzi https://orcid.org/0000-0002-1654-5211
Mpofana Sihoyiya https://orcid.org/0000-0003-1956-5223

REFERENCES

Bachmann, K., Osbahr, I., Tolosana-Delgado, R., Chetty, D. & Gutzmer, J. (2018) Variation in platinum group mineral and base metal sulfide assemblages in the Lower Group chromitites of the western Bushveld Complex, South Africa. *The Canadian Mineralogist*, 56, 723–743.

Barnes, S.-J., Maier, W.D & Ashwal, L.D. (2004) Platinum-group element distribution in the Main Zone and Upper Zone of the Bushveld Complex, South Africa. *Chemical Geology*, 208, 293–317.

Brodic, B., Malehmir, A. & Juhlin, C. (2017) Delineating fracture zones using surface-tunnel-surface seismic data, P-S and S-P mode conversions. *Journal of Geophysical Research. Solid Earth*, 122, 5493–5516. Available from: https://doi.org/10.1002/2017JB014304.

Brodic, B., Malehmir, A., Pacheco, N., Juhlin, C., Carvalho, J., Dynesius, L. et al. (2021) Innovative seismic imaging of volcanogenic massive sulfide deposits, Neves-Corvo, Portugal—Part 1: In-mine array. *Geophysics*, 86(3), B165–B179.

Campbell, G. (2011) Exploration geophysics of the Bushveld Complex in South Africa. *The Leading Edge*, 30, 622–638.

Cawthorn, R.G., Lee, C.A., Schouwstra, R.P. & Mellowship, P. (2002) Relationship between PGE and PGM in the Bushveld Complex. *The Canadian Mineralogist*, 40, 311–328.

Chistyakova, S., Latypov, R. & Youlton, K. (2019) Multiple Merensky Reef of the Bushveld Complex, South Africa. *Contributions to Mineralogy and Petrology*, 174, 26.

Kawohl, A. & Frimmel, H.E. (2016) Isoferroplatinum-pyrrhotite-troilite intergrowth as evidence of desulfurization in the Merensky Reef at Rustenburg (western Bushveld Complex, South Africa). *Mineralogical Magazine*, 80, 1041–1053.

Kinnaird, J.A. (2005) *The Bushveld large igneous province. Review paper*, vol. 39–45. Johannesburg, South Africa: The University of the Witwatersrand. Available from: http://www.largeigneousprovinces.org/sites/default/files/BushveldLIP.pdf [Accessed 17 January 2022].

Levander, A., Fuis, G.S., Wissinger, E.S., Lutter, W.J., Oldow, J.S. & Moore, T.E. (1994) Seismic images of the Brooks Range fold and thrust belt, Arctic Alaska, from an integrated seismic reflection/refraction experiment. *Tectonophysics*, 232(1–4), 13–30.

Lee, T., Chun, C. & Ryu, S.K. (2021). Detection of road-surface anomalies using a smartphone camera and accelerometer. *Sensors*, 21(2), 561.

Magalhães, N., Penniston-Dorland, S., Farquhar, J. & Mathez, E.A. (2018) Variable sulfur isotope composition of sulfides provide evidence for multiple sources of contamination in the Rustenburg Layered Suite, Bushveld Complex. *Earth and Planetary Science Letters*, 492, 163–173.

Magson, J., Tredoux, M. & Roelofse, F. (2018) Association of platinum-group elements with chromitite within the Merensky reef, Western Limb, Bushveld Complex: results of a high-resolution mineralogical and geochemical study. *Journal of African Earth Sciences*, 144, 161–175.

Malehmir, A., Durrheim, R., Bellefleur, G., Urosevic, M., Juhlin, C., White, D.J., Milkereit, B. & Campbell, G. (2012) Seismic methods in mineral exploration and mine planning, a general overview of past and present case histories and a look into the future. *Geophysics*, 77, WC173–WC190.

Malehmir, A., Maries, G., Bäckström, E., Schön, M. & Marsden, P. (2017) Developing cost-effective seismic mineral exploration methods using a landstreamer and a drophammer. *Scientific Reports*, 7, 10325.

Manzi, M.S, Hunt, E.J. & Durrheim, R.J. (2019) 3D reflection seismics for gold and platinum exploration, mine development and safety: case studies from the Witwatersrand Basin and Bushveld Complex (South Africa). In: Decrée,S& Robb,L (Eds.) *Ore deposits: origin, exploration, and exploitation. AGU geophysical monograph*, vol. 242. Hoboken, NJ: John Wiley & Sons, Inc., pp. 237–256.

Manzi, M.S.D., Cooper, G.R.J., Malehmir, A. & Durrheim, R.J. (2020) Improved structural interpretation of legacy 3D seismic data from Karee platinum mine (South Africa) through the application of novel seismic attributes. *Geophysical Prospecting*, 68, 145–163. Available from: https://doi.org/10.1111/1365-2478.12900.

Manzi, M.S.D., Gibson, M.A.S., Hein, K.A.A., King, N. & Durrheim, R.J. (2012) Application of 3D seismic techniques in evaluation of ore resources in the West Wits Line goldfield and portions of the West Rand goldfield, South Africa. *Geophysics*, 77, WC163–WC171.

Minato, S., Tsuji, T., Matsuoka, T., Nishizaka, N. & Ikeda, M. (2012) Global optimisation by simulated annealing for common reflection surface stacking and its application to low-fold marine data in southwest Japan. *Exploration Geophysics*, 43(2), 59–69.

Onyebueke, E.O., Durrheim, R.J., Manzi, M.S.D., Sebothoma, S., Zhang, S.E. & Stettler, E. (2020) High-resolution reflection seismic and electrical resistivity survey for an environmental purpose: a case study at Lancaster Gold Mine, Krugersdorp, South Africa. *Pure and Applied Geophysics*, 177(10), 4845–4870.

Onyebueke, E.O., Manzi, M.S.D. & Durrheim, R.J. (2018) High-resolution shallow reflection seismic integrated with other geophysical methods for hydrogeological prospecting in the Nylsvley Nature Reserve, South Africa. *Journal of Geophysics and Engineering*, 15(6), 2658–2673.

Oppermann, L., Junge, M., Schuth, S., Holtz, F., Schwarz-Schampera, U. & Sauheitl, L. (2017) Mobility and distribution of palladium and platinum in soils above Lower and Middle Group chromitites of the western Bushveld Complex, South Africa. *South African Journal of Geology*, 120, 511–524.

Riedel, M., Cosma, C., Enescu, N., Koivisto, E., Komminaho, K., Vaittinen, K. et al. (2018) Underground vertical seismic profiling with conventional and fiber-optic systems for exploration in the Kylylahti Polymetallic Mine, Eastern Finland. *Minerals*, 8(11), 538.

Royal Bafokeng Platinum (RBPlat). (2020) *RBPlat annual mineral resources and reserves statement 2020*. South Africa: Royal Bafokeng Platinum (RBPlat). Available from: https://www.bafokengplatinum.co.za/reports/integrated-report-2020/pdf/royal-bafokeng-platinum-mmr.pdf [Accessed 20 January 2022].

Sandmeier, K.J. (2020) *Reflexw 8.5 Manual, Sandmeier Software*. D-76227 Karlsruhe, Germany: Zipser Strabe 1.

Scheiber-Enslin, S.E. & Manzi, M. (2018) Integration of 3D reflection seismics and magnetic data for deep platinum mine planning and risk mitigation: a case study from Bushveld Complex, South Africa. *Exploration Geophysics*, 49(6), 928–939.

Schoenberg, R., Kruger, F.J., Nägler, T.F., Meisel, T. & Kramers, J.D. (1999) PGE enrichment in chromitite layers and the Merensky Reef of the western Bushveld Complex; a Re–Os and Rb–Sr isotope study. *Earth and Planetary Science Letters*, 172, 49–64.

Sheriff, R.E. & Geldart, L.P. (1995) *Exploration seismology*, 2nd edition, Cambridge: Cambridge University Press.

Stevenson, F., Higgs, R.M.A. & Durrheim, R.J. (2003) Seismic imaging of precious and base metal deposits in southern Africa. In: Eaton, D, Salisbury, M & Milkereit, B (Eds.) *Hardrock seismic exploration. Developments in geophysics series*. Houston: Society of Exploration Geophysicists, pp. 141–156.

Trickett, J.C., Düweke, W., Linzer, L., Kock, S. & Tootal, K. (2009, September) From *Aspirin* to '*The Bin*' in a *Mere* 85 *Years*: 11th SAGA Biennial Technical Meeting and Exhibition (pp. cp-241). European Association of Geoscientists & Engineers.

Westgate, M. & Manzi, M. (2017) Theoretical overview of complex seismic attributes: applications to soft and hard rock environments in South Africa. In: *International Geophysical Conference, 17–20 April 2017, Qingdao, China*. Society of Exploration Geophysicists and Chinese Petroleum Society, pp. 131–134.

Westgate, M., Manzi, M.S.D., James, I. & Harrison, W. (2020) New insights from legacy seismic data: reprocessing of legacy 2D seismic data for imaging of iron-oxide mineralization near Sishen Mine, South Africa. *Geophysical Prospecting*, 68(7), 2119–2140.

Yang, T., Wang, H., & Wang, X. (2021). Strain transfer characteristics of multi-layer optical fiber sensors with temperature-dependent properties at low temperature. *Sensors*, 21(2), 495.

Yilmaz, Ö. (2001) *Seismic data analysis*. Tulsa, OK: Society of Exploration Geophysicists.

Yilmaz, Ö. (2015) Engineering seismology with application to geotechnical engineering. In: *Investigations* in geophysics, vol. 17. Houston, TX: Society of Exploration Geophysics, pp. 162–512.

Zeh, A., Ovtcharova, M., Wilson, A.H. & Schaltegger, U. (2015) The Bushveld Complex was emplaced and cooled in less than one million years—Results of zirconology, and geotectonic implications. *Earth and Planetary Science Letters*, 418, 103–114.

How to cite this article: Onyebueke, E.O., Manzi, M.S.D., Rapetsoa, M.K., Kgarume, T., Westgate, M. & Durrheim, R.J. et al. (2024) Integration of in-mine seismic and GPR surveys to gain advanced knowledge of Bushveld Complex orebodies. *Near Surface Geophysics*, 22, 60–74. https://doi.org/10.1002/nsg.12270